Advanced Pharmaceutical Bulletin

Accepted Manuscript (unedited)

The manuscript will undergo copyediting, typesetting, and review of the resulting proof before it is published in its final form.

Research Article

How to cite this article:
Khosravi M, Ghotbeddin Z, Ghasemi-BabaAhmadi F. Hypoxia-Derived Exosomes and RNA-Binding Protein-Enriched Fractions Modify Inflammatory Responses in Normal Microglial Cells. Advanced Pharmaceutical Bulletin, doi: 10.34172/apb.47409

Hypoxia-Derived Exosomes and RNA-Binding Protein-Enriched Fractions Modify Inflammatory Responses in Normal Microglial Cells

Mohammad Khosravi[a*], Zohreh Ghotbeddin[b], Fatemeh Ghasemi-BabaAhmadi[c]

[a] Department of Pathobiology, Faculty of Veterinary Medicine, Shahid Chamran University of Ahvaz, Ahvaz, Iran
[b] Department of Basic Sciences, Faculty of Veterinary Medicine, Shahid Chamran University of Ahvaz, Ahvaz, Iran
[c] Faculty of Veterinary Medicine, Shahid Chamran University of Ahvaz, Ahvaz, Iran

ARTICLE INFO

Keywords:
Microglia,
Hypoxia,
Inflammation,
Exosome,
RNA binding proteins

Article History:
Submitted: May 07, 2026
Revised: August 01, 2026
Accepted: August 14, 2026
ePublished: September 07, 2026

ABSTRACT

Purpose: Brain hypoxia triggers neuroinflammatory responses that are partly mediated by microglia and their secreted exosomes. This study investigated whether hypoxia-derived microglial exosomes and RNA-binding protein (RBP)-enriched fractions are associated with alterations in the inflammatory phenotype of healthy microglial cells.

Methods: Neonatal Wistar rats were randomly assigned to four groups (n = 5/group): control (C), hypoxia (H), one-week post-hypoxia (HW1), and age-matched one-week control (CW1). Brain tissues and primary microglia were collected to isolate exosomes and RBP-enriched fractions. RBP-enriched fractions were obtained using RNA-conjugated Fe nanoparticles linked by EDC-NHS chemistry and subsequently incorporated into microglial exosomes. Healthy primary microglial cells were treated with exosomes, RBP-enriched fractions, or exosome-loaded RBP-enriched fractions (20 µg/mL; five biological replicates per treatment). Assessments included cell viability, expression of inflammatory and anti-inflammatory genes, innate immune responses, and exosome biodistribution.

Results: Microglia-derived exosomes showed preferential accumulation in brain tissue following systemic administration. Treatment by exosomes from the hypoxia group were associated with increased microglial viability and elevated expression of inflammatory markers 24 hours post-treatment. In contrast, exosomes containing hypoxia-derived RBP-enriched fractions were associated with increased ratio of TGF-β/TNF-α and CD206/CD80 expression and reduced expression of CD80, IL-1β, and NOX2 compared with their respective exosome controls. In innate immune assays, RBP-HW1 significantly reduced antiprotease activity, while RBP-H significantly decreased lysozyme and myeloperoxidase activities.

Conclusion: These findings suggest that the biological effects of microglial exosomes depend on the physiological state of the donor cells, and that hypoxia-derived RBP-enriched fractions are associated with the modulation of inflammatory responses in recipient microglia. However, because the RBP-enriched fractions were not characterized by mass spectrometry or specific immunoblotting, and mechanistic intervention experiments were not conducted, the responsible molecular components

***Corresponding Author**
Mohammad Khosravi, Email: m.khosravi@scu.ac.ir, ORCID: 0000-0001-9510-3464

Introduction

Brain ischemia and hypoxia are among the most common consequences of impaired cerebral blood circulation and metabolic dysfunction, affecting both humans and animals across different stages of life. Cerebral hypoxia can severely impair cognitive and behavioral functions and is associated with the development of numerous neurological disorders.[1] In response to hypoxic injury, resident innate immune cells, particularly microglia, together with infiltrating immune cells such as mast cells and lymphocytes, release a broad range of pro-inflammatory mediators. Concurrently, axonal and myelin damage, accompanied by the loss of oligodendrocyte precursor cells, mature oligodendrocytes, and neurons, activates multiple intracellular signaling pathways that contribute to disease progression.[2]

Pathophysiological conditions including inflammation, tissue injury, infection, ischemia, cancer, and severe hypoxia profoundly influence immune cell function. Under these conditions, excessive immune activation may exacerbate tissue damage, promote tumor progression, and contribute to autoimmune disorders. A central mechanism underlying these responses is the transcriptional regulation mediated by hypoxia-inducible factors (HIFs), which coordinate both innate and adaptive immune responses.[3–5] Activation of the HIF signaling pathway directly stimulates the expression of numerous pro-inflammatory cytokines in both hypoxic and neighboring normoxic cells, thereby amplifying inflammatory responses.[6]

Neuronal survival and function depend on the precise regulation of gene expression. This process is controlled by multiple regulatory mechanisms, including hormonal signaling, transcription factor activity, chromatin remodeling, and RNA-dependent pathways such as post-transcriptional regulation, RNA transport, nuclear trafficking, and mRNA stabilization. Many of these processes are orchestrated by RNA-binding proteins (RBPs).[7] Beyond their established roles in RNA metabolism, RBPs regulate mRNA transport, translation, and microRNA (miRNA) biogenesis, making them essential coordinators of cellular homeostasis. Given their broad regulatory functions, dysregulation of RBP expression or activity can disrupt neuronal integrity and has been implicated in the pathogenesis of numerous neurodegenerative and autoimmune diseases.[7]

Exosomes are nanosized extracellular vesicles secreted by nearly all cell types and have emerged as important mediators of intercellular communication. They transport a diverse array of biologically active molecules, including proteins, DNA, and various RNA species, thereby influencing the physiological and pathological states of recipient cells.[8,9] Their low immunogenicity, intrinsic biocompatibility, and ability to cross the blood-brain barrier make exosomes particularly attractive candidates for targeted drug delivery and therapeutic applications in neurological disorders.[10]

Intercellular communication mediated by exosomes plays a fundamental role in brain repair following injury. Exosomes released from neural cells regulate the interactions between microglia and other resident brain cells, thereby influencing the neuroinflammatory response. During brain injury, classically activated microglia (M1) promote inflammation through the production of pro-inflammatory mediators, whereas alternatively activated microglia (M2) facilitate inflammation resolution, neurogenesis, and tissue repair.[11] Consequently, understanding the mechanisms governing microglial polarization has become a major focus in the development of therapeutic strategies for ischemic stroke and other neurological disorders.[12]

Although exosomes can exert neuroprotective effects by delivering beneficial biomolecules to injured tissues, exosomes released from hypoxic neurons have also been reported to activate microglia and promote neuroinflammation.[13] Hypoxia-induced activation of the NF-κB signaling pathway and subsequent nuclear translocation of this transcription factor stimulate the expression of numerous pro-inflammatory genes, thereby amplifying inflammatory responses.[14] Moreover, hypoxic stress promotes the polarization of microglia toward the M1 phenotype, which further accelerates neuronal damage. Therefore, interventions capable of modulating microglial polarization during hypoxia may represent promising therapeutic approaches for limiting neuroinflammation and reducing secondary brain injury.[15]

In our previous study, we investigated the roles of exosomes and RBP-enriched fraction in cellular resistance to hypoxia and demonstrated that several RBPs exert protective effects in hypoxic microglial cells. Specifically, hypoxic stress induced the expression of multiple protective RBPs, suggesting their involvement in adaptive responses to oxygen deprivation.[16] Building upon these findings, the present study aimed to determine whether these protective proteins accumulate within microglia and whether exosomes serve as vehicles for their transfer to neighboring cells, thereby modulating inflammatory responses and microglial differentiation. We further compared the biological activities of RBPs and exosomes isolated from hypoxic microglia to clarify their respective contributions to microglial polarization. To test this hypothesis, exosomes and RBPs-enriched fractions were isolated from microglial cells and brain tissues obtained from four experimental groups: rats subjected to acute hypoxia (H), rats examined one week after hypoxia during the recovery phase (HW1), and their respective age-matched control groups (C and CW1). The effects of these exosomal and protein fractions on microglial differentiation and inflammatory responses were subsequently evaluated.

Materials and Methods

Animals

Pregnant Wistar rats (n = 6) were obtained from Jundishapur University of Medical Sciences, Ahvaz, Iran. Before transportation, all cages were thoroughly sanitized to minimize the risk of microbial contamination. Neonatal Wistar rats (10–12 days old, 20 ± 5 g) were housed under standard laboratory conditions with free access to food and water, appropriate bedding, controlled temperature, and a 12 h light/dark cycle.

The pups were randomly allocated into four experimental groups (n = 5 per group): hypoxia (H), one week after hypoxia (HW1), hypoxia control (C), and one week after hypoxia control (CW1).

Hypoxia was induced using a custom-made glass chamber supplied with a gas mixture containing 7% oxygen and 93% nitrogen. Neonatal rats were exposed to the hypoxic atmosphere for 30 min daily over five consecutive days. Oxygen concentration was continuously monitored using an oxygen meter, while the chamber temperature and relative humidity were maintained at 23 ± 1°C and 40–50%, respectively.

Animals in the H and C groups were euthanized 24 h after the final hypoxic exposure, whereas animals in the HW1 and CW1 groups were euthanized one week later. Euthanasia was performed by high dose ketamine/xylazine injection and cervical dislocation followed by sterile blood collection, after which brain tissues were immediately harvested for subsequent analyses.

Preparation of Fe–RNA Conjugates and Isolation of RNA-Binding Proteins

RBPs-enriched fractions were isolated using magnetic iron oxide nanoparticles conjugated with total RNA, as previously described with minor modifications.[16] Briefly, five neonatal rats were euthanized at 7 days of age, and total RNA was extracted from brain tissue using a commercial RNA extraction kit (Sinaclon, Iran) according to the manufacturer's instructions. RNA integrity was verified by agarose gel electrophoresis, while purity and concentration were determined spectrophotometrically by measuring the A260/A280 ratio. The RNA concentration was adjusted to 40 µg/mL.

Magnetic iron oxide nanoparticles bearing surface amino groups were synthesized according to the method described by Khosravi et al.[17] Briefly, 20 µg of purified RNA was dissolved in 1 mL of 10 mM MES buffer, followed by the sequential addition of 100 µL EDC (4 mg/mL) and 100 µL NHS (6 mg/mL). The reaction mixture was incubated for 30 min to activate the RNA for covalent coupling. Subsequently, 100 µL of activated magnetic nanoparticles (OD600 = 0.312) was added, and the suspension was gently shaken for 2 h at room temperature to allow conjugation.

The Fe–RNA conjugates were collected magnetically and resuspended in 0.1 M Tris buffer (pH 8.0) prepared in MES buffer to quench residual reactive groups. After a further 2 h incubation, the nanoparticles were collected again and resuspended in PBS or PBS supplemented with 1% bovine serum albumin and 5 µL RNase inhibitor.

Successful RNA conjugation was confirmed using Fourier-transform infrared spectroscopy (FTIR; PerkinElmer 2400), ultraviolet-visible (UV–Vis) spectroscopy at 260 nm (Nabi, Microdigital Co., Ltd., South Korea), and field-emission scanning electron microscopy (FESEM) (MIRA 2, Tescan, Czech Republic), as previously reported.[17] The average diameters of the magnetic iron oxide (Fe_3O_4) nanoparticles and the Fe–RNA conjugates were determined by measuring 10 randomly selected particles from each sample using the image analysis software integrated with the FESEM microscope.

For isolation of RBPs-enriched fraction, 1 g of homogenized pooled brain tissue obtained from hypoxic or control animals was incubated with the prepared Fe–RNA conjugates for 1 h at room temperature under continuous agitation. Following magnetic separation, the particles were washed five times until no detectable protein remained in the supernatant. RNA-bound proteins were subsequently eluted using 0.1 M Tris buffer (pH 8.0) at 55°C and collected after magnetic separation of the nanoparticles. The isolated proteins were analyzed by SDS–PAGE and quantified using the Bradford protein assay in three independent samples from each experimental group.

The hydrodynamic diameter and zeta potential of the magnetic nanoparticles, RNA, and Fe–RNA conjugates were determined in PBS (pH 7.2) using dynamic light scattering (DLS) and electrophoretic light scattering with a Zetasizer (Version 7.03, Malvern Panalytical Ltd.; Serial No. 1094694).

Microglial Cell Isolation and Culture

Primary microglial cells were isolated and cultured according to the method described by Woolf et al. (2025).[18] Neonatal rats of the all groups (n=5) were euthanized by an overdose of ketamine-xylazine and cervical dislocation, and the brains were immediately removed and transferred to cold Dulbecco's Modified Eagle Medium (DMEM). Under a stereomicroscope, the meninges were carefully removed, and the cerebral cortex and hippocampus were dissected. Half of the brain tissue was stored at −70°C for subsequent analyses, while the remaining tissue was minced into small fragments in serum-free DMEM. Tissue dissociation was performed by incubation with trypsin for 15 min, after which fetal bovine serum (FBS) was added to terminate enzymatic digestion. The cell suspension was centrifuged at 1,000 rpm for 3 min, and the resulting supernatant was transferred to a new tube and centrifuged again at 3,000 rpm for 5 min. The final cell pellet was resuspended in complete culture medium and seeded into FBS-coated T-75 culture flasks. Cells were maintained in a humidified incubator at 37°C with 5% CO_2. Four hours after seeding, the culture medium was replaced to remove non-adherent cells and cellular debris. The adherent microglial cells were subsequently maintained under standard culture conditions until they reached the desired stage for experimentation.

Isolation and Characterization of Microglial-Derived Exosomes

Twenty-four hours after establishing the microglial cultures, the culture medium was removed, and the cells were washed twice with phosphate-buffered saline (PBS). Serum-free DMEM (5 mL) was then added, and the cells were incubated for an additional 24 h to allow exosome secretion. Conditioned medium was collected and centrifuged at 3,000 × *g* for 15 min to remove cellular debris. The supernatant was subsequently filtered through a 0.20-μm membrane filter, and exosomes were isolated using a commercial precipitation kit (ExoCib, Iran) according to the manufacturer's instructions. Protein concentrations of the isolated exosomes were determined using the Bradford assay. Protein profiles of both exosome preparations and isolated RBPs were analyzed by SDS-PAGE. Exosomes obtained from hypoxic and control microglia were processed separately throughout all experiments.

For morphological characterization, 50 μL of each exosome suspension was deposited onto aluminum substrates and allowed to air-dry for 1 h. Samples were fixed with 2% paraformaldehyde and sequentially dehydrated using graded acetone solutions (30%, 40%, 50%, 60%, 70%, 80%, 90%, and 100%), with a 10-min incubation at each concentration. The samples were then examined using a FESEM microscope. The average diameters of exosomes derived from the microglial cells of the hypoxic and control groups were determined by measuring 10 randomly selected particles from each sample using the image analysis software integrated with the FESEM microscope.

Exosomal surface marker expression was evaluated by flow cytometry. Exosome samples (4 μg) were suspended in 49 μL of PEB buffer (PBS containing 5 mM EDTA and 0.5% bovine serum albumin). APC-conjugated anti-CD63, PE-conjugated anti-CD9, and FITC-conjugated anti-CD81 monoclonal antibodies (Miltenyi Biotec, Germany) were added, and samples were incubated for 1 h at 4°C in the dark. Following incubation, samples were diluted with 450 μL of PEB buffer and analyzed by flow cytometry. Fluorochrome-matched isotype antibodies served as negative controls.

The hydrodynamic diameter and zeta potential of the isolated exosomes were measured in PBS (pH 7.2) using a Zetasizer (Version 7.03, Malvern Panalytical Ltd.).

Loading of Hypoxia-Associated RNA-Binding Proteins into Exosomes

Fluorescein labeling of hypoxia-associated RBPs-enriched fractions, purification of labeled proteins, and exosome loading were performed according to our previously reported protocol.[16] Briefly, 1 µL of FITC solution (5 mg/mL) was activated using EDC/NHS chemistry in 10 mM MES buffer. Subsequently, 40 µg of purified RBP-enriched fraction was added and incubated for 1 h under gentle agitation to allow covalent conjugation. The reaction was terminated by adding 1.5 M Tris buffer (pH 8.8) to achieve a final concentration of 0.1 M. Unreacted FITC molecules were removed by dialysis against PBS at 4°C for 48 h.

Purified FITC-labeled RBPs were subsequently loaded into exosomes using the suspension-loading method. Briefly, isolated exosomes were transiently permeabilized with carbonate buffer (pH 9.6) and incubated with the labeled RBPs for 1 h at room temperature. Loaded exosomes were then recovered using the ExoCib precipitation kit according to the manufacturer's protocol and used for subsequent experiments.

Biodistribution of Microglial-Derived Exosomes

To evaluate the in vivo biodistribution of microglial-derived exosomes, 200 µL of exosome suspension (50 µg/mL) loaded with FITC-labeled RBPs was administered intravenously through the tail vein of healthy Wistar rats (n = 4). An additional four untreated animals served as negative controls.

Twenty-four hours after administration, the animals were euthanized, and the brain, lungs, liver, kidneys, spleen, and heart were carefully excised and placed individually in Petri dishes. Ex vivo fluorescence imaging was performed using a KODAK FX Pro Imaging System. Images were acquired in fluorescence mode with an exposure time of 3 min using excitation and emission wavelengths of 470 and 535 nm, respectively. Fluorescence signals emitted from each organ were captured, digitized, and analyzed using the integrated imaging software.

Cell Viability Assay

The effects of exosomes, isolated RBPs-enriched fraction, and RBP-loaded exosomes on microglial viability, polarization, and cytokine expression were evaluated in vitro**.** Protein concentrations of all preparations were quantified using the Bradford assay and normalized before treatment.

Primary microglial cells were detached from T-75 culture flasks using trypsin, counted, and seeded into 96-well culture plates at approximately 5×10^3 cells per well. After 48 h of incubation, cells were treated with exosomes isolated from the C, H, CW1, and HW1 groups, the corresponding RBP-enriched fractions, or exosomes loaded with their respective RBPs. All treatment groups received a final protein concentration of 20 µg/mL in 100 µL of DMEM. Control wells received culture medium alone. Each experimental condition was performed with at least five biological replicates.

After 24 h of treatment, a subset of cultures was harvested for immunological analyses and real-time PCR. The remaining cultures were maintained for either one or two weeks to assess long-term cell viability. Cells were cultured at 37°C in a humidified atmosphere containing 5% CO_2, and the culture medium was replaced every 72

h. During the second week, detached cells were recovered by centrifugation (2,000 rpm, 4 min) and returned to their respective wells to minimize cell loss.

Cell viability was determined using the MTT assay. MTT reagent was prepared at a concentration of 5 mg/mL in DMEM, and 100 µL was added to each well. Following incubation for 4 h at 37°C, the MTT solution was removed, and the resulting formazan crystals were dissolved in 100 µL of dimethyl sulfoxide (DMSO). Plates were incubated for an additional 30 min in the dark, after which absorbance was measured at 600 nm using a microplate reader.

Quantitative Real-Time PCR Analysis

Following 24 h of treatment, the culture medium was removed, and the cells were washed twice with PBS. Cells were detached using 30 µL of trypsin for 5 min, and enzymatic activity was terminated by adding 200 µL of DMEM. The cell suspension was collected into microcentrifuge tubes and centrifuged at 2,000 rpm for 5 min.

Total RNA was subsequently extracted, and the expression levels of inflammatory and anti-inflammatory markers, including Arginase-1 (Arg1), gp91phox (NOX2), TNF-α, TGF-β, IL-1β, CD80, and CD206, were quantified by quantitative Real Time PCR. β-Actin was used as the internal housekeeping gene for normalization. Primer sequences are listed in Table 1. Gene expression analysis was performed 24 h after treatment of the microglial cells. Each Real Time-PCR reaction was carried out in a final volume of 20 µL containing 10 µL of 2× Master Mix (Amplicon, Germany), 1 µL of each forward and reverse primer (Table 1), 2 µL of cDNA template, and nuclease-free water to the final volume. Reaction mixtures were prepared in 3 replicates on ice and amplified using a StepOnePlus™ Real-Time PCR System (Applied Biosystems, USA). The thermal cycling conditions consisted of an initial denaturation at 94°C for 5 min, followed by 35 amplification cycles of 95°C for 30 s, 60°C for 30 s, and 72°C for 30 s. A final extension step was performed at 72°C for 8 min.

Table 1. The gene sequences of the rat primers for Real-Time PCR analysis

Gene	´3→ 5 Forward Primer Sequences ´5→ 3 Reverse Primer Sequences	Sequence length	Reference
TNF-a	F: TGCCTCAGCCTCTTCTCATTC R: GCTCCTCCGCTTGGTGGTTT	217	Sun et al., 2020 [11]
TGF-β	F: CTTCAGCTCCACAGAGAAGAACTGC R: CACGATCATGTTGGACAACTGCTCC	298	Nakagawa et al., 2018 [19]
IL-1β	F: GCAGGACTTTAAGGGTTACTTGG R: GGGGAGAAATCGATGACAGC	82	O'Bryan et al., 2004 [20]
CD80	F: TGGTGCTGGCTG GTCTTTC R: CTGTGCCACTTCTTTCACTTCC	156	Satoh et al., 2002 [21]
CD206	F: GACGGACGAGGAGTTCATTATAC R: GTTGGAGAGATAGGCACAGAAG	88	Hirosawa et al., 2018 [22]
Arginase-1	F: CCAGTATTCACCCCGGCTAC	198	Hirosawa et al., 2018 [22]

	R: ACAAGACAAGGTCAACGCCA		
NADPH.gp91	F: CTGCCAGTGTGTCGGAATCT R : TGTGAATGGCCGTGTGAAGT	142	Aryafar et al., 2021[23]
B-actin	F: TCCTTCCTGGGTATGGAATC R : GCACTGTGTTGGCATAGAGG	103	Zhu et al., 2009 [24]

Evaluation of Innate Immune Responses

Lysozyme Activity

Lysozyme activity was determined using *Micrococcus lysodeikticus* as the substrate. Briefly, a suspension containing 2 mg of *M. lysodeikticus* in 10 mL of 0.02 M acetate buffer (pH 5.5) was prepared. Cell lysate (20 µL) (n=5 per group) was mixed with 80 µL of the bacterial suspension in a 96-well microplate, and absorbance was measured at 600 nm after 5 min. A decrease in absorbance of 0.001 OD/min was fits to 1 mL per minutes and defined as one unit of lysozyme activity.[25]

Myeloperoxidase Activity

Myeloperoxidase (MPO) activity was measured according to the modified method of Malle et al.[26] Briefly, 10 µL of cell lysate (n=5 per group) was mixed with 90 µL of calcium- and magnesium-free Hanks' balanced salt solution in 96-well plates. Tetramethylbenzidine (TMB; 20 mM) and hydrogen peroxide (H_2O_2; 5 mM) were then added as reaction substrates. After incubation for 5 min at room temperature, the reaction was terminated with 35 µL of 4 M sulfuric acid. MPO activity was determined by measuring absorbance at 450 nm using a microplate reader.

Antiprotease Activity

Antiprotease activity was determined according to the method described by Ellis.[27] Briefly, 20 µL of 5% trypsin was mixed with 100 µL of 50 mM Tris-HCl buffer (pH 8.2), followed by the addition of 10 µL of cell lysate (n=5 per group). Control wells (n=5) contained all reagents except the cell lysate. After incubation for 1 h at room temperature, the substrate Nα-benzoyl-DL-arginine *p*-nitroanilide (BAPNA; 0.1 mM) and calcium chloride (20 mM) were added to initiate the reaction. Absorbance was measured at 405 nm before and after an additional 30-min incubation at room temperature. Antiprotease activity was calculated as the reduction in trypsin activity relative to the control samples.

Statistical Analysis

Each experiment was performed independently at least three times unless otherwise specified. Statistical analyses were conducted using SPSS software (Version 2022; IBM Corp., Armonk, NY, USA). Data normality was assessed using the Shapiro–Wilk test, and homogeneity of variances was evaluated using the Brown–Forsythe test. When the assumptions of normality were not met, comparisons were performed using the Wilcoxon rank-sum test. Comparisons among multiple groups were performed using one-way analysis of variance (ANOVA), followed by Tukey's post hoc multiple-comparison test. Graphs were generated using GraphPad Prism version 8

(GraphPad Software, San Diego, CA, USA). A *P* value < 0.05 was considered statistically significant. Data are presented as the mean ± standard deviation (SD). Relative gene expression was analyzed using the comparative Ct ($2^{-\Delta\Delta Ct}$) method implemented in StepOne™ software. The ΔΔCt value was calculated according to the following equation:

ΔΔCt = (Ct_target − Ct_β-actin) sample − (Ct_target − Ct_β-actin) control

Relative expression levels were expressed as fold changes ($2^{-\Delta\Delta Ct}$). Data are presented as the mean ± standard deviation (SD). Differences were considered statistically significant at $P < 0.05$. The results of the innate immune assays were normalized according to the total protein concentration of each cell sample

Results

Hypoxia Induction

Body weight of the neonates were monitored throughout the hypoxia induction period to evaluate the physiological effects of oxygen deprivation. Repeated exposure to hypoxia resulted in a significant reduction in body weight compared with the control group (F(9,30) = 14.1). Weight loss became evident on the second day after hypoxia induction (*P* = 0.02) and progressed further on the fourth and fifth days (*P* = 0.0005) (Figure 1A).

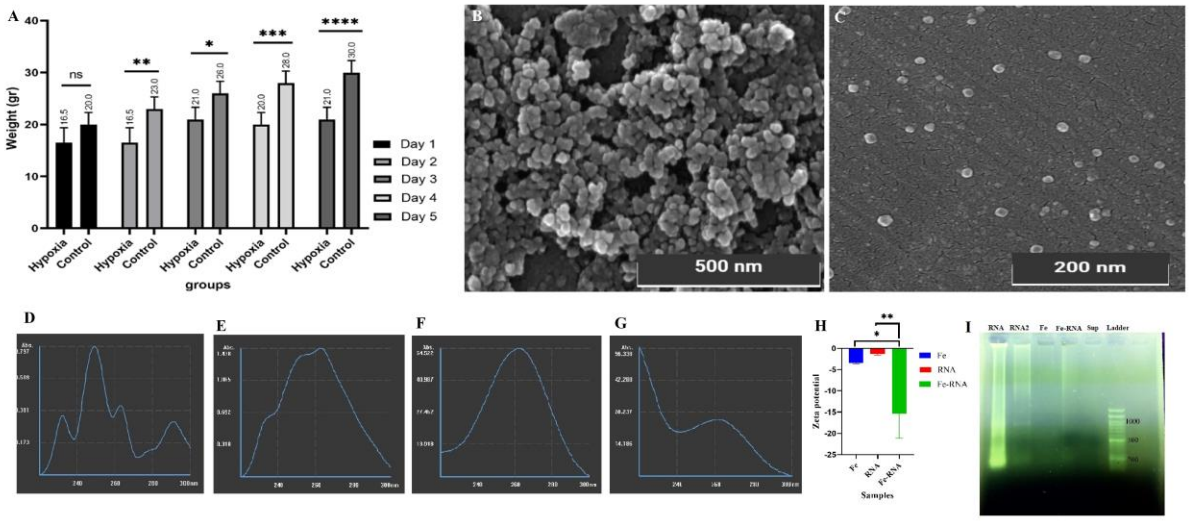

Figure 1.

Preparation and Characterization of Fe–RNA Conjugates

RNA was successfully conjugated to magnetic Fe nanoparticles using EDC/NHS-mediated coupling. The morphology of the nanoparticles before and after conjugation was examined by field-emission scanning electron microscopy (FESEM) (Figures 1B and 1C). Conjugation with RNA significantly increased the average particle size from 29.35 ± 4.20 nm for unconjugated Fe nanoparticles to 50.74 ± 17.90 nm for Fe–RNA conjugates (*P* = 0.014, F = 18.41, DFn = 5).

Ultraviolet-visible (UV–Vis) spectroscopy demonstrated successful RNA conjugation by detecting the characteristic absorbance at 260 nm. Based on the method described above, the conjugation efficiency was estimated to be approximately 45% (Figures 1D–G).

The surface charge of the Fe–RNA conjugates also differed significantly from that of both unconjugated Fe nanoparticles (P = 0.01) and free RNA (P = 0.004) ($F(2,6) = 15$), indicating successful surface modification (Figure 1H). Agarose gel electrophoresis further supported RNA conjugation, as Fe-RNA conjugate exhibited a diffuse smear pattern rather than the distinct migration observed for free RNA (Figure 1I).

In addition, Fourier-transform infrared (FTIR) spectroscopy, as reported in our previous study,[16] further verified successful RNA immobilization on the Fe nanoparticles. Compared with unconjugated components, the Fe–RNA conjugates exhibited the disappearance of the amide I band, an increase in the intensity of the amide II band, and the loss of characteristic phosphate (P=O) and carbonyl absorption bands of RNA, consistent with interactions between RNA functional groups and the nanoparticle surface.

Characterization of RNA-Binding Proteins and Microglial-Derived Exosomes

The concentration of RBPs fractions isolated from brain tissues differed significantly among the experimental groups ($F(3,12) = 11.61$, P = 0.0007). The highest RBP concentration was detected in the one-week post-hypoxia (HW1) group (60.80 μg/mL), which was significantly greater than that of the control (C; 29.66 μg/mL, P = 0.001), acute hypoxia (H; 30.41 μg/mL, P = 0.0015), and one-week control (CW1; 38.58 μg/mL, P = 0.013) groups. Owing to the relatively low abundance of individual RBPs, proteins present at low concentrations were not readily identified by SDS-PAGE.

Protein quantification of brain-derived exosomes also revealed significant differences among the experimental groups. The mean protein concentrations of exosome preparations obtained from the C, H, HW1, and CW1 groups were 140.70, 62.42, 88.14, and 108.89 μg/mL, respectively. Exosomes isolated from the control group contained significantly higher protein levels than those isolated from the H (P = 0.0008) and CW1 (P = 0.013) groups ($F(3,8) = 14.79$, P = 0.0013).

The size distribution of exosomes was analyzed by dynamic light scattering (DLS) (Figures 2A–D). The principal particle size detected in the control group was smaller than that observed in the H, CW1, and HW1 groups. However, no significant differences were detected among the H, CW1, and HW1 groups. Analysis of zeta potential demonstrated significant differences among the experimental groups ($F(3,8) = 4.021$, P = 0.046). Specifically, exosomes isolated from the HW1 group exhibited a significantly higher zeta potential than those from the control group (Figure 2E).

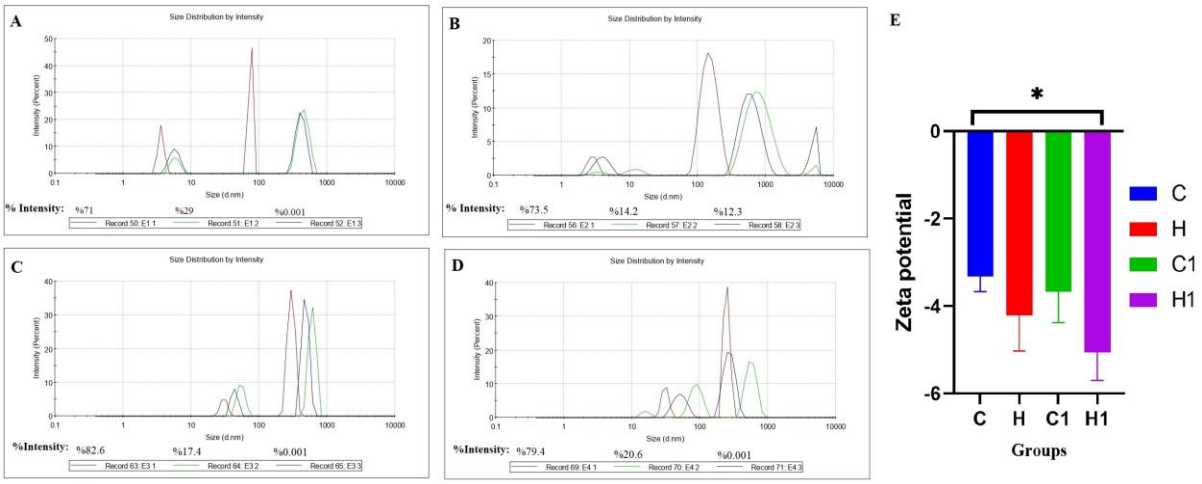

Figure 2. Dynamic light scattering (DLS) and zeta potential analysis of isolated exosomes. Size distribution profiles of exosomes isolated from the (A) control (C), (B) hypoxia (H), (C) one-week control (CW1), and (D) one-week post-hypoxia (HW1) groups. (E) Zeta potential measurements of exosomes isolated from microglial cells in the corresponding experimental groups.

Primary microglial cells exhibited characteristic morphological changes during culture. On the first day, cells displayed a predominantly spherical morphology. Between days 3 and 5, they gradually acquired a spindle-shaped appearance, followed by a marked increase in proliferation between days 7 and 9. By day 9, most cells exhibited branched processes with well-defined extensions, consistent with the morphology of cultured microglia (Figure 3A).

Morphological analysis of isolated exosomes by FESEM showed no significant difference in particle diameter between the control and hypoxia groups (F = 2.116, DFn = 9, P = 0.28). Nevertheless, exosomes isolated from hypoxic microglia exhibited a modest increase in mean diameter (150.63 nm) compared with those isolated from control cells (139.28 nm) (Figures 3B and 3C).

The identity of the isolated extracellular vesicles was further verified by analysis of the exosomal surface markers CD9, CD63, and CD81 (Figure 3D). Consistent with our previous findings,[16] exosomes isolated from hypoxic microglia exhibited significantly higher expression of all three tetraspanin markers than those isolated from control cells, confirming successful isolation of exosome-enriched vesicles.

Biodistribution of Microglial-Derived Exosomes

The tissue distribution of FITC-labeled microglial-derived exosomes was evaluated by ex vivo fluorescence imaging 24 h after intravenous administration. Organ-specific uptake was quantified by normalizing fluorescence intensity to the corresponding organ area. As shown in Figures 3E and 3F, exosomes exhibited a significantly greater accumulation in the brain than in untreated control animals (F(3,12) = 5.306, P = 0.027). In contrast, fluorescence signals detected in the lungs, liver, spleen, kidneys, and heart did not differ significantly from those of the control group, indicating minimal uptake by these organs.

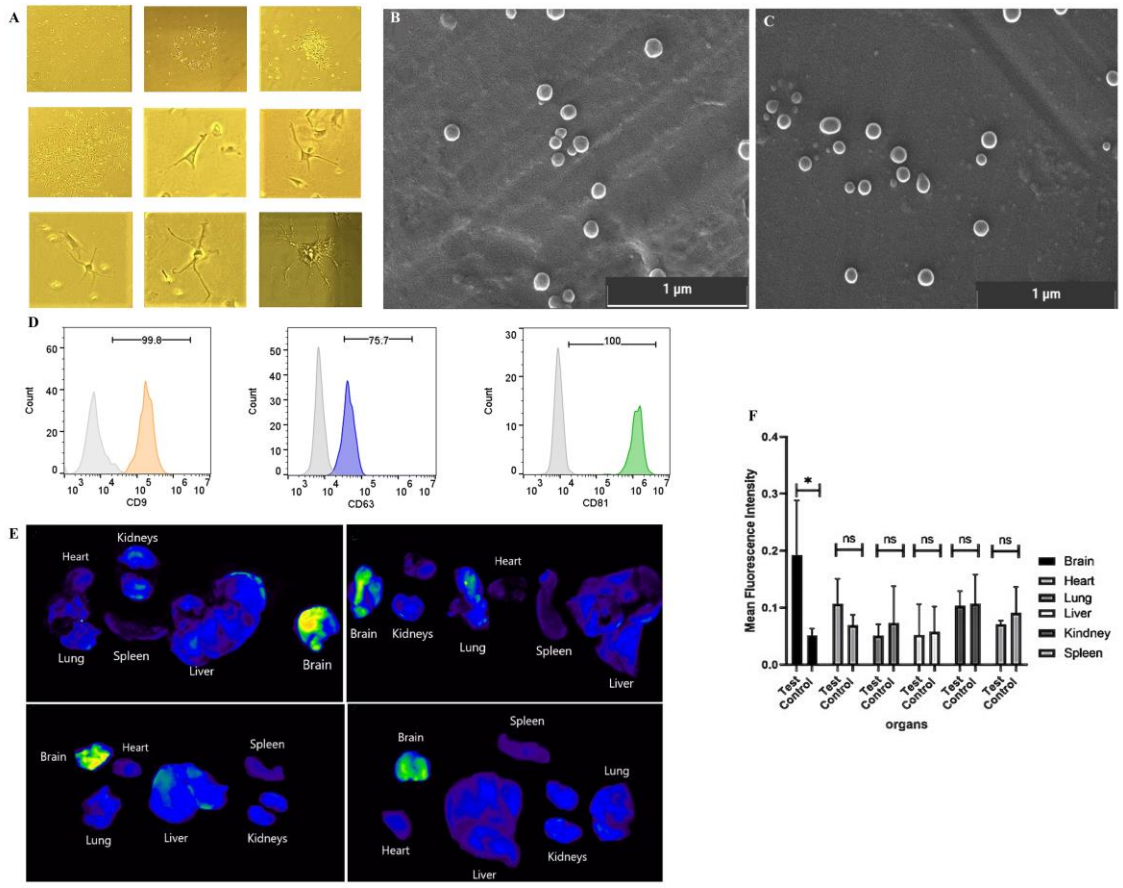

Figure 3. Biodistribution and characterization of microglial-derived exosomes. (A) Representative images showing morphological changes of primary microglial cells during the 9-day culture period. Cells gradually acquired a ramified morphology, with the majority exhibiting mature microglial characteristics between days 7 and 9. (B, C) FESEM images showing the morphology and size of exosomes isolated from control (B) and hypoxic (C) microglia. (D) Expression of the exosomal markers CD9, CD63, and CD81 in exosomes isolated from the control and hypoxia groups. (E) Representative ex vivo fluorescence images of the brain, lungs, liver, spleen, kidneys, and heart collected 24 h after intravenous administration of FITC-labeled exosomes. (F) Quantitative analysis of fluorescence intensity demonstrating preferential accumulation of microglial-derived exosomes in the brain. Groups with different lowercase letters differ significantly ($P < 0.05$).

Effects of Exosomes, RNA-Binding Proteins, and RBP-Loaded Exosomes on Microglial Viability

Microglial viability following treatment with exosomes, RBPs-enriched fraction, or RBP-loaded exosomes (EXO-RBP) was assessed using the MTT assay and compared with untreated control cells.

Treatment with exosomes significantly affected microglial viability in a time-dependent manner (Figures 4A–C). Twenty-four hours after treatment, exosomes derived from the hypoxia group (H) significantly increased cell viability compared with untreated controls ($F(4,15) = 11.32$, $P = 0.0002$; H vs. control, $P = 0.0026$) (Figure 4A).

After 7 days, treatment with exosomes isolated from the one-week control (CW1) and one-week post-hypoxia (HW1) groups significantly reduced cell viability relative to untreated controls ($F(4,15) = 6.617$, $P = 0.0028$; CW1, $P = 0.0051$; HW1, $P = 0.0039$) (Figure 4B).

In contrast, after 14 days, microglial viability was significantly higher in cells treated with exosomes from the C, H, and CW1 groups than in untreated cells ($F(4,15) = 7.11$, $P = 0.002$; C, $P = 0.0027$; H, $P = 0.0127$; CW1, $P = 0.0042$) (Figure 4C).

Treatment with isolated RBPs-enriched fraction produced a different temporal response (Figures 4D–F). No significant differences in cell viability were observed 24 h after treatment ($F(4,15) = 0.680$, $P = 0.616$) (Figure 4D). However, after 7 days, RBPs-enriched fraction isolated from the control (RBP-C) and hypoxia (RBP-H) groups significantly reduced cell viability compared with untreated cells ($F(4,14) = 6.284$, $P = 0.0041$; RBP-C, $P = 0.004$; RBP-H, $P = 0.013$) (Figure 4E). By day 14, treatment with RBP-C and RBP-HW1 significantly increased cell viability relative to untreated controls ($F(4,15) = 3.869$, $P = 0.0236$; RBP-C, $P = 0.036$; RBP-HW1, $P = 0.024$) (Figure 4F).

Unlike exosomes or RBPs-enriched fraction alone, treatment with RBP-loaded exosomes (EXO-RBP) did not significantly alter microglial viability at any of the evaluated time points, including day 1 ($F(4,15) = 1.416$, $P = 0.2766$), day 7 ($F(4,15) = 0.326$, $P = 0.85$), or day 14 ($F(4,15) = 0.213$, $P = 0.926$) (Figures 4G–I).

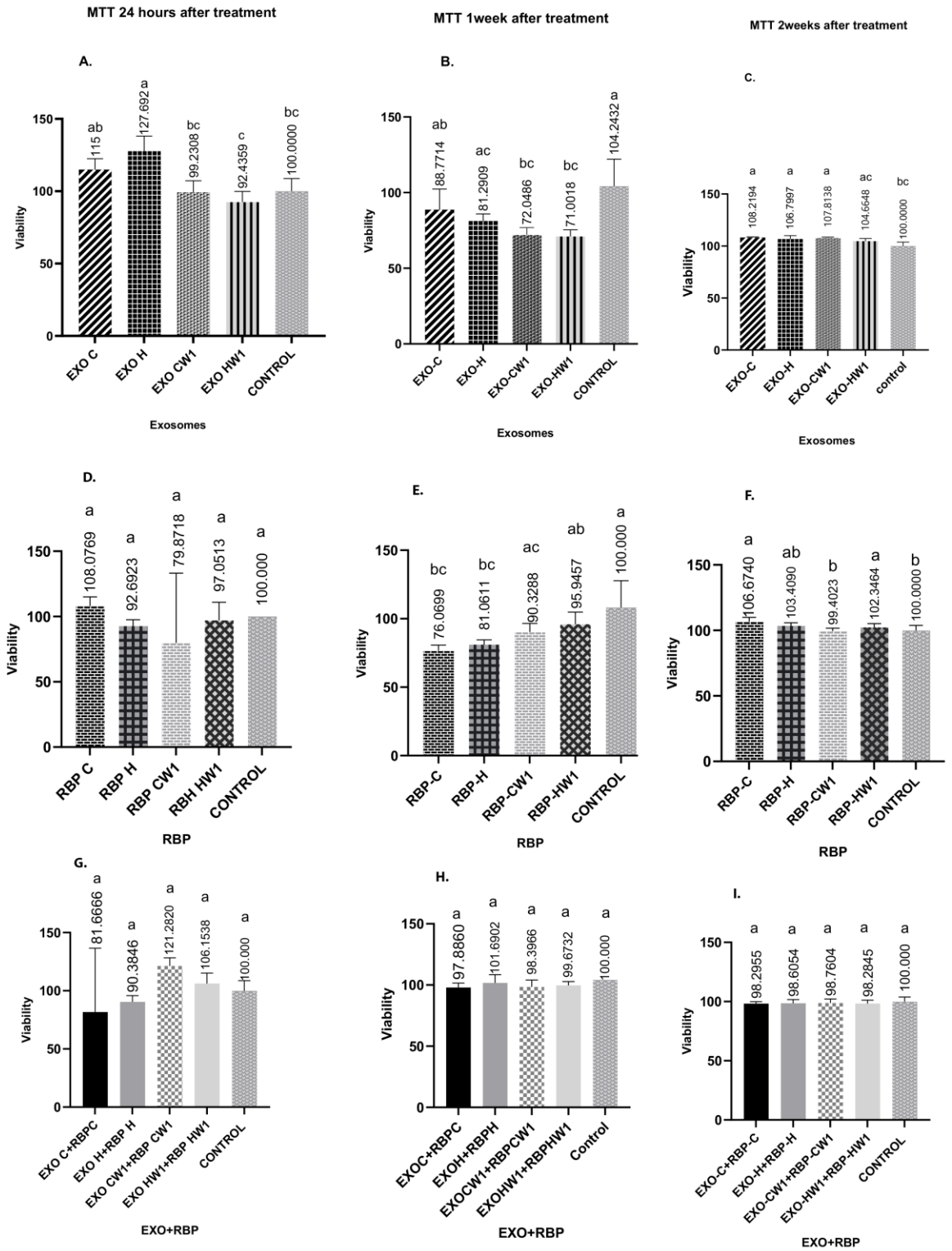

Figure 4. Effects of exosomes, RBPs-enriched fraction, and RBP-loaded exosomes (EXO-RBP) on microglial viability. Exosomes and RBPs-enriched fraction were isolated from the control (C), hypoxia (H), one-week post-hypoxia (HW1), and one-week control (CW1) groups. (A–C) Cell viability measured 1, 7, and 14 days after treatment with exosomes. (D–F) Cell viability following treatment with isolated RBPs-enriched fraction at the corresponding time points. (G–I) Cell viability following treatment with RBP-loaded exosomes (EXO-RBP). Cell viability was normalized to untreated control cells, which were defined as 100% viability at each time point. Different lowercase letters indicate statistically significant differences among groups ($P < 0.05$).

Expression of Inflammatory and Anti-Inflammatory Genes

The effects of vehicle exosomes and RBP-loaded exosomes (EXO-RBP) on microglial inflammatory responses were evaluated by quantitative real-time PCR analysis of genes associated with pro-inflammatory and anti-inflammatory phenotypes. Relative expression levels of CD80, CD206, TNF-α, TGF-β, IL-1β, NOX2 (gp91phox), and Arginase-1 are summarized in Figure 5.

Treatment with control-derived exosomes (Exo-C) markedly increased the expression of CD80 (30.8-fold), CD206 (4.2-fold), TGF-β (34.2-fold), and TNF-α (53.5-fold) relative to untreated microglial cells (Figures 5A–D).

Microglia treated with exosomes isolated from the hypoxia group (Exo-H) exhibited even greater induction of CD80 (53.2-fold) and CD206 (44.1-fold). In addition, expression of TGF-β, TNF-α, and IL-1β increased by 2.5-, 16.2-, and 10.6-fold, respectively (Figures 5A–E).

In contrast, treatment with exosomes isolated from the HW1 and CW1 groups produced only minor changes in gene expression, with all evaluated genes exhibiting less than threefold variation compared with untreated controls (Figure 5).

Distinct expression profiles were observed following treatment with RBP-loaded exosomes. Exosomes loaded with RBP-C induced marked increases in CD80 (54.3-fold), CD206 (26.9-fold), TGF-β (28.8-fold), TNF-α (13.1-fold), and NOX2 (11.1-fold) expression (Figures 5A–F).

Treatment with Exo-CW1 loaded with RBP-CW1 resulted in the greatest induction of Arginase-1 (240.6-fold), accompanied by increased expression of TGF-β (43.5-fold) and CD206 (8.6-fold). More moderate increases were also observed for TNF-α (6.8-fold) and NOX2 (5.4-fold) (Figures 5B–G).

Microglia treated with Exo-H loaded with RBP-H displayed increased expression of CD80 (11.7-fold), CD206 (39.6-fold), and TGF-β (10.9-fold), whereas TNF-α expression increased only modestly (1.3-fold) (Figures 5A–D).

Similarly, treatment with Exo-HW1 loaded with RBP-HW1 increased the expression of CD80 (11.8-fold), CD206 (5.4-fold), TGF-β (53.7-fold), and NOX2 (27.1-fold) compared with untreated microglial cells (Figures 5A, 5B, 5D, and 5F).

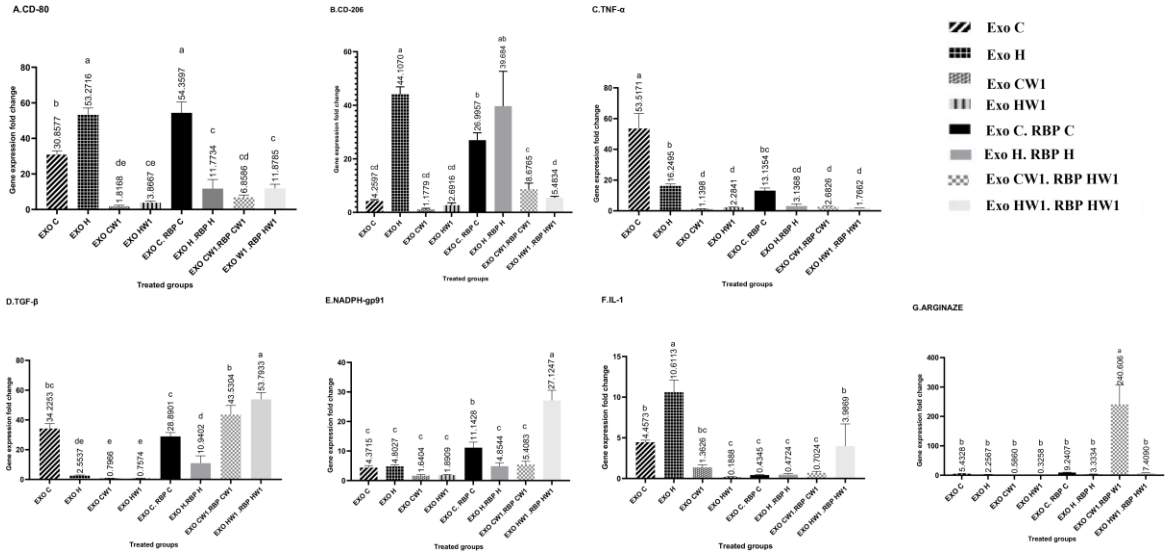

Figure 5. Relative expression of inflammatory- and anti-inflammatory-associated genes in microglial cells following treatment with vehicle exosomes or RNA-binding protein-loaded exosomes (EXO-RBP). Expression levels of (A) CD80, (B) CD206, (C) TNF-α, (D) TGF-β, (E) IL-1β, (F) NOX2 (gp91phox), and (G) Arginase-1 were determined by quantitative real-time PCR. Exo-C, Exo-H, Exo-CW1, and Exo-HW1 represent exosomes isolated from the corresponding experimental groups, whereas EXO-RBP denotes exosomes loaded with the corresponding RNA-binding proteins. Relative expression was calculated using the $2^{-\Delta\Delta Ct}$ method with β-actin as the internal reference gene. Different lowercase letters indicate statistically significant differences among groups ($P < 0.05$).

Innate Immune Responses

The effects of exosomes, RBPs-enriched fraction, and RBP-loaded exosomes (EXO-RBP) on innate immune responses were evaluated by measuring antiprotease, lysozyme, and myeloperoxidase (MPO) activities (Figure 6).

Antiprotease Activity

Significant differences in antiprotease activity were observed among the treatment groups ($F(12,26) = 30.01$, $P < 0.0001$). Treatment with RBP-HW1 resulted in the lowest antiprotease activity compared with all other experimental groups ($P < 0.0001$). Similarly, exosomes loaded with RBP-HW1 significantly reduced antiprotease activity ($P = 0.0007$). In contrast, exosomes loaded with RBP-H and RBP-CW1 exhibited significantly higher antiprotease activity than untreated control cells (Figure 6A).

Lysozyme Activity

Lysozyme activity also differed significantly among the treatment groups ($F(12,26) = 15.82$, $P < 0.0001$). Cells treated with RBP-H displayed significantly lower lysozyme activity than the remaining groups ($P = 0.0139$). Conversely, treatment with EXO-RBP-HW1 ($P = 0.0003$), RBP-C ($P = 0.0002$), RBP-CW1 ($P < 0.0001$), Exo-CW1 ($P = 0.0053$), and Exo-H ($P = 0.0140$) significantly increased lysozyme activity relative to untreated controls (Figure 6B).

Myeloperoxidase Activity

Myeloperoxidase (MPO) activity was significantly affected by the different treatments ($F(12,26) = 34.38$, $P < 0.0001$). Compared with untreated microglia, significantly higher MPO activity was observed following treatment with Exo-C ($P < 0.0001$), Exo-H ($P = 0.0021$), Exo-CW1 ($P < 0.0001$), Exo-HW1 ($P = 0.0021$), RBP-C ($P < 0.0001$), RBP-CW1 ($P < 0.0001$), RBP-HW1 ($P = 0.0016$), EXO-RBP-C ($P < 0.0001$), and EXO-RBP-CW1 ($P = 0.0002$) (Figure 6C).

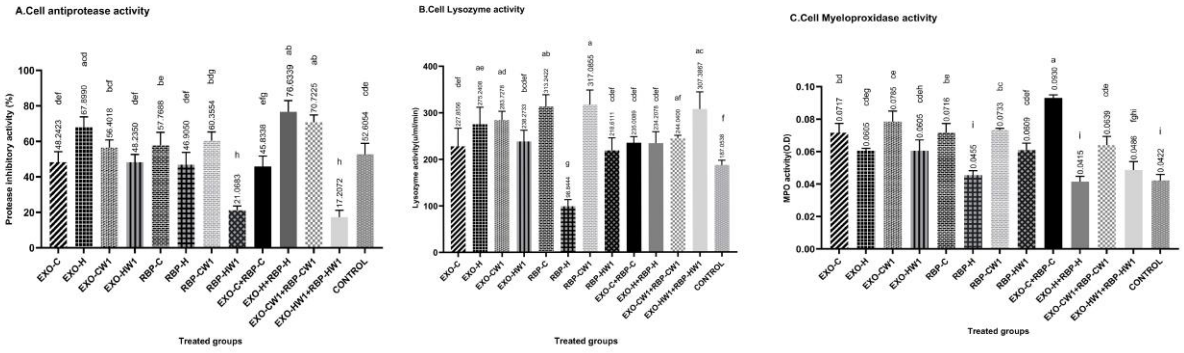

Figure 6. Effects of exosomes, RBPs-enriched fractions, and RBP-loaded exosomes (EXO-RBP) on innate immune responses in microglial cells. (A) Antiprotease activity, (B) lysozyme activity, and (C) myeloperoxidase (MPO) activity following treatment with samples derived from the control (C), hypoxia (H), one-week control (CW1), and one-week post-hypoxia (HW1) groups. Different lowercase letters indicate statistically significant differences among treatment groups ($P < 0.05$).

Discussion

Appropriate regulation of inflammatory responses is essential for maintaining microglial homeostasis and normal central nervous system function. Although the molecular mechanisms responsible for microglial activation have been extensively investigated, considerably less is known about the processes that terminate inflammation and restore immune homeostasis. Exosomes have emerged as important mediators of intercellular communication and may function either as distress signals released by injured cells or as regulators that promote the resolution of inflammation. Accordingly, one of the primary objectives of the present study was to investigate the role of microglia-derived exosomes in transmitting hypoxia-associated signals and modulating inflammatory responses in recipient microglial cells.

Previous studies have shown that exosomes derived from hypoxic mesenchymal stem cells promote functional recovery following spinal cord injury by facilitating the polarization of microglia from a pro-inflammatory to a reparative phenotype.[28] In contrast, our findings demonstrate that exosomes released from hypoxic microglia exert markedly different biological effects. Specifically, treatment of healthy microglial cells with hypoxia-derived exosomes markedly increased the expression of the pro-inflammatory markers CD80 and IL-1β, accompanied by reduced TGF-β expression, indicating that exosomes originating from hypoxic microglia propagate inflammatory signals rather than suppress them. These findings suggest that the biological activity of exosomes is highly dependent on the physiological state and cellular origin of the donor cells.

Consistent with our previous observations, exosome size remained within the expected range (approximately 50–150 nm) and did not differ significantly among the experimental groups. In contrast, hypoxic conditions altered several other exosomal characteristics. Although hypoxia increased exosome release, the protein content of

individual exosome preparations was reduced, which may reflect diminished cellular viability or altered exosome biogenesis under hypoxic stress. Furthermore, our previous study demonstrated increased expression of the canonical exosomal markers CD9, CD63, and CD81 in exosomes isolated from hypoxic microglia.[16]

The physicochemical properties of extracellular vesicles, particularly particle size and zeta potential, are influenced by multiple technical factors, including the isolation method, storage conditions, buffer composition, and measurement conditions.[29,30] Because these variables were carefully standardized across all experimental groups, the observed differences in zeta potential are more likely to reflect biological alterations in exosomal membrane composition than methodological variation. Notably, the increase in zeta potential became more pronounced during the recovery phase one week after hypoxia, suggesting that hypoxic injury induces persistent remodeling of the exosomal membrane. Such changes may involve alterations in membrane lipid composition, sialylation, or membrane-associated proteins, although these possibilities require further biochemical investigation.

Microglial polarization has emerged as an attractive therapeutic target for neurological disorders characterized by excessive neuroinflammation. Several experimental approaches, including IL-4, interferon regulatory factor 7 (IRF7), miR-124, and chitinase-1, have been shown to promote the transition of microglia toward a reparative phenotype and improve outcomes in experimental models of central nervous system injury.[31-34] Our findings extend this concept by identifying hypoxia-associated RBPs as previously unrecognized modulators of microglial polarization. In particular, exosomes loaded with RBPs isolated during the recovery phase preferentially enhanced the expression of anti-inflammatory markers, including Arginase-1, CD206, and TGF-β, while producing a distinct transcriptional profile compared with exosomes alone. These observations suggest that RBPs may contribute to the regulation of microglial phenotypic plasticity following hypoxic injury.

Collectively, the present findings indicate that hypoxia modifies both the molecular cargo and the biological activity of microglial-derived exosomes. Whereas exosomes released during acute hypoxia predominantly promoted pro-inflammatory signaling, the incorporation of hypoxia-associated RBPs substantially altered the transcriptional responses of recipient microglia, suggesting that these proteins participate in shaping the inflammatory phenotype after hypoxic injury. Further studies are warranted to identify the individual RBPs responsible for these effects and to determine whether modulation of exosomal RBP cargo represents a feasible therapeutic strategy for the treatment of hypoxia-associated neuroinflammatory disorders.

Previous studies have shown that exosomes can exert either beneficial or detrimental biological effects depending on the physiological state of their donor cells and the molecular composition of their cargo. Exosomes released under pathological conditions may contain elevated levels of glutamate, viral proteins, or pro-inflammatory cytokines, thereby contributing to cellular injury and the propagation of inflammation. In contrast, microglia-derived exosomes have also been reported to promote neurite outgrowth, enhance neuronal survival following hypoxic injury, and support metabolic recovery in neural tissues.[35] These observations underscore the context-dependent nature of exosome-mediated signaling.

In the present study, no significant changes in the viability of healthy microglial cells were detected 24 h after treatment with either exosomes or RBP-loaded exosomes, indicating that these treatments did not induce acute cytotoxicity. Although treatment with isolated RBPs reduced cell viability after one week, this effect was not

observed when the same proteins were delivered within exosomes. These findings suggest that the primary biological effects of exosomes and RBPs are related to modulation of cellular metabolism and functional phenotype rather than the direct induction of cell death. Consistent with this interpretation, our previous study demonstrated that exosomes isolated from the CW1 group enhanced the viability of hypoxic microglial cells.[16] Furthermore, exosomes derived from microglia under different physiological conditions elicited distinct inflammatory and anti-inflammatory transcriptional responses in recipient cells. Collectively, these findings indicate that the physiological state of the donor microglia influences the biological activity of their released exosomes. Consequently, assessment of inflammatory gene expression provides a more informative measure of exosome-mediated functional changes than cell viability alone.

Another important finding of this study is the preferential accumulation of microglia-derived exosomes within brain tissue following systemic administration. Consistent with previous reports, exosome uptake is highly selective and depends on both the donor and recipient cell types. For example, neuron-derived exosomes are preferentially internalized by neighboring neurons, whereas microglia efficiently internalize extracellular vesicles released from neurons, astrocytes, oligodendrocytes, and other microglia.[36] This selective uptake is largely mediated by membrane-associated molecules, including lipids, integrins, tetraspanins, glycoproteins, and other surface ligands that regulate cell-specific recognition.

The preferential localization of microglia-derived exosomes to the brain observed in the present study further supports their physiological role in intercellular communication within the central nervous system and highlights their potential as targeted delivery vehicles for therapeutic molecules. Nevertheless, several challenges remain before exosome-based therapies can be translated into clinical practice. Native exosomes may carry donor-derived immunogenic molecules, including major histocompatibility complex (MHC) proteins, particularly MHC class I molecules, which could trigger immune responses in allogeneic recipients. Therefore, strategies aimed at reducing the immunogenicity of exosomal cargo or engineering exosomes with improved biocompatibility will likely be required for their safe therapeutic application.

Our findings also suggest that hypoxia-associated RBPs may represent promising therapeutic candidates independent of the exosomal carrier. Because many RBPs are highly conserved and function as central regulators of post-transcriptional gene expression, they may provide a novel strategy for modulating microglial activation and inflammatory responses after hypoxic brain injury.[37-39] Future studies should identify the individual RBPs responsible for these effects and define the molecular pathways through which they regulate microglial phenotype and neuroinflammation.

RBPs are key regulators of post-transcriptional gene expression that influence RNA processing, stability, transport, localization, and translation.[40] Eukaryotic cells express a large and diverse repertoire of RBPs, each characterized by distinct RNA-binding specificities and protein–protein interaction networks. Throughout evolution, these regulatory networks have become increasingly complex, enabling RBPs to coordinate cellular metabolism and adaptive responses to environmental stress. Like many signaling proteins, RBPs are regulated not only at the transcriptional level but also through post-translational modifications that influence their activity, localization, and interactions with RNA.[41]

The present study expands the current understanding of RBP function by demonstrating that RBP-enriched fractions isolated from hypoxic brain tissue modulate inflammatory gene expression in recipient microglial cells. These findings complement our previous work, in which hypoxia-associated RBPs enhanced the expression of genes involved in cellular adaptation to hypoxia, including HIF-1α, VEGF-A, protein disulfide isomerase (PDI), and carboxypeptidase E (CPE).[16] Together, these observations suggest that RBPs participate in coordinating multiple adaptive responses to hypoxic stress, including both metabolic adaptation and regulation of neuroinflammation.

RBPs are also increasingly recognized as important regulators of innate and adaptive immune signaling through their ability to control mRNA stability, translation, and degradation.[41] By selectively regulating inflammatory transcripts, RBPs enable cells to rapidly adjust gene expression in response to changes in the local microenvironment. The present findings indicate that hypoxia-associated RBPs modify the expression of both pro-inflammatory and anti-inflammatory mediators, supporting their involvement in regulating microglial activation following hypoxic injury.

Activated microglia play a central role in the neuroinflammatory response by releasing mediators such as TNF-α, IL-1β, reactive oxygen species (ROS), and other inflammatory factors. Conversely, they can promote tissue repair by producing cytokines including IL-4, IL-10, and TGF-β.[42] In the present study, treatment with Exo-C loaded with RBP-C produced a transcriptional profile characterized by increased expression of several pro-inflammatory markers. In contrast, exosomes carrying RBP-H or RBP-CW1 preferentially enhanced the expression of genes associated with anti-inflammatory or reparative responses, particularly TGF-β, CD206, and Arginase-1. Although these findings suggest that hypoxia-associated RBPs influence the balance of inflammatory signaling, the specific proteins responsible for these effects remain unknown. Identification of these individual RBPs and characterization of their molecular targets should be a priority for future investigations.

Reactive oxygen species generated by NADPH oxidases are known to play important roles in both tissue injury and repair following cerebral hypoxia. Vermot et al. demonstrated that hypoxic conditions activate NOX2 and NOX4, thereby increasing ROS production and enhancing VEGFR2-dependent angiogenic signaling.[43] In agreement with this concept, the highest NOX2 expression observed in the present study occurred in microglia treated with Exo-HW1 containing RBP-HW1. Rather than simply indicating oxidative damage, this increase may reflect activation of signaling pathways involved in vascular remodeling and tissue repair during recovery from hypoxic injury. Nevertheless, additional functional studies will be required to distinguish between the detrimental and reparative roles of NOX signaling in this context.

Persistent neuroinflammation following hypoxia has been reported previously. Ziemka-Nalecz et al. demonstrated that inflammatory responses are initiated within minutes after hypoxic injury and may persist for weeks or even months.[2] Consistent with these observations, the present study identified sustained alterations in inflammatory gene expression following exposure to hypoxia-associated exosomes and RBPs. However, prolonged changes in microglial viability were not observed, possibly because the biological activity of the transferred proteins diminished over time owing to protein turnover and intracellular degradation.

The biological effects of individual cytokines should also be interpreted within the context of the overall inflammatory network. For example, TNF-α can promote cell survival and proliferation through activation of TNF

receptor 2 (TNFR2) and the Akt signaling pathway, whereas excessive TNF-α signaling through TNF receptor 1 (TNFR1) activates caspase-dependent apoptotic pathways. Consequently, evaluation of individual cytokines in isolation may not accurately reflect the functional state of microglia. Comprehensive profiling of inflammatory mediators, together with pathway-level analyses, is therefore likely to provide a more accurate assessment of microglial activation and the mechanisms through which RBPs regulate neuroinflammatory responses.

Transforming growth factor-β1 (TGF-β1) is a key regulator of immune homeostasis in the central nervous system and plays an important role in limiting excessive inflammation following brain injury. Increased TGF-β1 expression promotes the acquisition of reparative microglial phenotypes and contributes to tissue repair after hypoxic or ischemic insults. In addition to its anti-inflammatory functions, TGF-β1 regulates several downstream genes involved in inflammatory signaling and tissue remodeling, including COX-2, IL-6, and NOX4.[44] Li et al. demonstrated that both TGF-β1 and its receptors (TGFβRI and TGFβRII) are highly expressed in the developing brain and are further upregulated following hypoxic injury.[45] Consistent with these observations, the present study showed marked induction of TGF-β expression following treatment with Exo-C and EXO-RBP-CW1. These findings suggest that both exosomal cargo and hypoxia-associated RBP-enriched fractions contribute to the regulation of signaling pathways involved in maintaining microglial homeostasis and promoting recovery after hypoxic stress.

Arginine metabolism has emerged as an important determinant of microglial function during neuroinflammation. Increased expression of Arginase-1 shifts arginine metabolism away from nitric oxide production and has frequently been associated with tissue repair and the resolution of inflammation. Chen et al. reported that arginine supplementation reduced neuronal loss following cerebral ischemia and attenuated inflammatory responses in cultured microglia.[46] Similarly, increased arginase expression has been observed in the cortex, hippocampus, and infiltrating macrophages following hypoxic brain injury.[9,47] In the present study, the highest Arginase-1 expression was detected in microglia treated with EXO-RBP-HW1 and EXO-RBP-CW1. These findings suggest that RBP-enriched fractions isolated during the recovery phase preferentially activate molecular pathways associated with tissue repair and inflammatory resolution.

The expression patterns of CD206, TGF-β, CD80, and TNF-α further support the concept that hypoxia-associated exosomal cargo modulates microglial activation rather than producing a simple binary transition between inflammatory states. CD206, the macrophage mannose receptor, is widely recognized as a marker associated with reparative microglial functions, including phagocytosis and tissue remodeling.[48] In the present study, increased CD206 expression closely paralleled TGF-β expression, whereas elevated CD80 expression was generally accompanied by increased TNF-α, consistent with previous reports describing inflammatory activation of microglia and macrophages.[31] Importantly, the simultaneous expression of both inflammatory and reparative markers observed in several treatment groups suggests a dynamic or transitional activation state rather than a strictly polarized phenotype, reflecting the complexity of microglial responses following hypoxic injury.

Functional analyses of innate immune responses were consistent with the transcriptional findings. Exosomes derived from hypoxic microglia significantly increased lysozyme and myeloperoxidase activities in recipient microglial cells, whereas hypoxia-associated RBP-enriched fractions partially attenuated these responses,

particularly by reducing lysozyme activity. Moreover, exosomes isolated from the C and CW1 groups produced distinct innate immune responses despite both being derived from non-hypoxic animals. These differences likely reflect developmental changes occurring during the early postnatal period, when both the central nervous system and the innate immune system undergo rapid maturation.[49,50] Consequently, the biological activity of exosomes appears to depend not only on pathological stimuli such as hypoxia but also on the developmental stage of the donor cells.

Collectively, our findings indicate that the physiological state of donor microglia profoundly influences both the molecular composition and the biological activity of their released exosomes. Acute hypoxia generates exosomes that preferentially amplify inflammatory signaling, whereas RBP-enriched fractions obtained during the recovery phase promote transcriptional programs associated with inflammatory regulation and tissue repair. These observations identify hypoxia-associated RBPs as potential modulators of microglial function and suggest that engineering the molecular cargo of exosomes, or selectively targeting exosome-mediated communication after hypoxic injury, may represent promising therapeutic strategies for limiting neuroinflammation while preserving endogenous repair mechanisms.

Limitations

This study has several limitations that should be considered when interpreting the findings. First, the RBP-enriched fractions isolated using RNA-conjugated Fe nanoparticles were neither characterized by mass spectrometry nor validated by immunoblotting for canonical RBPs. Consequently, the specific protein components responsible for the observed biological effects remain unidentified, and the potential contribution of co-isolated proteins cannot be entirely excluded. Second, although the study demonstrated significant associations between hypoxia-derived exosomes, RBP-enriched fractions, and alterations in microglial inflammatory responses, no mechanistic intervention experiments, such as inhibition of exosome uptake or knockdown of specific RBPs, were conducted to establish causal relationships. Finally, comprehensive characterization of exosomal cargo, including proteomic and transcriptomic profiling, was beyond the scope of this study.

Future studies should identify individual RBPs and other bioactive exosomal components using high-resolution proteomic techniques, such as liquid chromatography-tandem mass spectrometry (LC-MS/MS), complemented by targeted immunoblot validation. Functional analyses employing gain- and loss-of-function approaches, along with inhibition of exosome uptake, will be essential to elucidate the molecular pathways underlying the observed effects. Addressing these limitations will provide a more comprehensive understanding of exosome-mediated communication during brain hypoxia and will better establish the therapeutic potential of hypoxia-associated, RBP-enriched fractions in neuroinflammatory and neurodegenerative disorders.

Conclusion

The present study demonstrates that both microglia-derived exosomes and RBP-enriched fractions influence microglial function following hypoxic injury. Although these treatments produced only limited effects on cell viability, they markedly altered the expression of genes associated with inflammatory and reparative responses. Exosomes released from hypoxic microglia promoted a transcriptional profile characterized by increased expression of pro-inflammatory markers, whereas exosomes carrying hypoxia-associated RBP-enriched fractions

shifted gene expression toward a more regulatory phenotype, with enhanced expression of molecules such as TGF-β, CD206, and Arginase-1. These findings indicate that the biological activity of microglial exosomes is strongly influenced by the physiological state of the donor cells and by the molecular composition of their cargo.

Our results further suggest that hypoxia-associated RBP-enriched fractions modulate inflammatory signaling in recipient microglia and may contribute to the regulation of neuroinflammatory responses during recovery from hypoxic injury. Rather than supporting a simple transition between discrete microglial phenotypes, the observed transcriptional changes are consistent with dynamic modulation of microglial activation, reflecting the complexity of inflammatory regulation within the central nervous system. Collectively, this study identifies hypoxia-associated RBP-enriched fractions as previously unrecognized modulators of exosome-mediated intercellular communication in the brain and provides new insight into the molecular mechanisms underlying microglial responses to hypoxia. Future studies should identify the individual RBPs responsible for these biological effects using proteomic approaches, including mass spectrometry, and investigate how specific exosomal cargo components regulate microglial signaling and neuroinflammation. Such studies may facilitate the development of engineered exosome-based therapeutics or RBP-targeted strategies for the treatment of hypoxia-associated neurological disorders and other neurodegenerative diseases.

Ethics approval

All tests on animals were carried out in accordance with animal protection laws and guidelines of research ethics committee of Shahid Chamran University of Ahvaz approved with verification code of IR.SCU. REC.1402.017.

Consent for publication

Not applicable

Funding

This study was financially supported by the Shahid Chamran University of Ahvaz, Ahvaz, Iran with grant number of SCU.VP1403.12470.

CRediT authorship contribution statement

Khosravi M: Writing – review and editing, Writing original draft, Validation, Methodology, Investigation, Formal analysis, Data curation, Conceptualization. **Ghotbeddin Z**: Investigation, Formal analysis, Data curation, Conceptualization, Writing – review & editing. **Ghasemi-BabaAhmadi. F:** Investigation, Formal analysis, Writing original draft.

Declaration of interest

The authors declare that they have no conflict of interest.

Acknowledgment

The authors thank Dr. Ali Bashiri Dezfouli and Dr. Ehsan Pipelzdeh for their kind consultation.

Data availability

All analyzed and raw data are available on the Zenodo website at the following address: https://doi.org/10.5281/zenodo.20936751.

References

1. Tarkowska A. Hypoxic-Ischemic Brain Injury after Perinatal Asphyxia as a Possible Factor in the Pathology of Alzheimer's Disease. Exon Publications 2021:45-59. doi: 10.36255/exonpublications.cerebralischemia.2021.perinatalasphyxia

2. Ziemka-Nalecz M, Jaworska J, Zalewska T. Insights into the neuroinflammatory responses after neonatal hypoxia-ischemia. J Neuropathol Exp Neurol. 2017;76(8):644-54. doi: 10.1093/jnen/nlx046

3. Chang G, Leu J-S, Ma L, Xie K, Huang S. Methylation of RNA N6-methyladenosine in modulation of cytokine responses and tumorigenesis. Cytokine. 2019;118:35-41. doi: 10.1016/j.cyto.2018.06.018

4. Chen Y, Gaber T. Hypoxia/HIF modulates immune responses. Biomedicines. 2021;9(3):260. doi: 10.3390/biomedicines9030260

5. Mitroshina EV, Savyuk MO, Ponimaskin E, Vedunova MV. Hypoxia-inducible factor (HIF) in ischemic stroke and neurodegenerative disease. Front Cell Dev Biol. 2021;9:703084. doi: 10.3389/fcell.2021.703084

6. Malkov MI, Lee CT, Taylor CT. Regulation of the hypoxia-inducible factor (HIF) by pro-inflammatory cytokines. Cells. 2021;10(9):2340. doi: 10.3390/cells10092340

7. Parra AS, Johnston CA. Emerging roles of RNA-binding proteins in neurodevelopment. J Dev Biol. 2022;10(2):23. doi: 10.3390/jdb10020023

8. Graner MW, Alzate O, Dechkovskaia AM, Keene JD, Sampson JH, Mitchell DA, et al. Proteomic and immunologic analyses of brain tumor exosomes. FASEB J. 2009 May;23(5):1541. doi: 10.1096/fj.08-122184

9. Mathivanan S, Fahner CJ, Reid GE, Simpson RJ. ExoCarta 2012: database of exosomal proteins, RNA and lipids. Nucleic Acids Res. 2012;40(D1):D1241-D4. doi: 10.1093/nar/gkr828

10. Shetgaonkar GG, Marques SM, DCruz CE, Vibhavari R, Kumar L, Shirodkar RK. Exosomes as cell-derivative carriers in the diagnosis and treatment of central nervous system diseases. Drug Deliv Transl Res. 2022;12(5):1047-79. doi: 10.1007/s13346-021-01026-0

11. Sun H, He X, Tao X, Hou T, Chen M, He M, et al. The CD200/CD200R signaling pathway contributes to spontaneous functional recovery by enhancing synaptic plasticity after stroke. J Neuroinflammation. 2020;17(1):171. doi: 10.1186/s12974-020-01845-x

12. Wang Y, Huang K, Qin Z, Zeng J, Zhang Y, Yin L, et al. Ultraprecise real-time monitoring of single cells in tumors in response to metal ion-mediated RNA delivery. ACS Appl Mater Interfaces. 2022;14(33):37291-300. doi: 10.1021/acsami.2c06306

13. Jiang H, Zhao H, Zhang M, He Y, Li X, Xu Y, et al. Hypoxia induced changes of exosome cargo and subsequent biological effects. Front Immunol. 2022;13:824188. doi: 10.3389/fimmu.2022.824188

14. Jiang R-H, Xu J-J, Zhu D-C, Li J-F, Zhang C-X, Lin N, et al. Glycyrrhizin inhibits osteoarthritis development through suppressing the PI3K/AKT/NF-κB signaling pathway in vivo and in vitro. Food Funct. 2020;11(3):2126-36. doi: 10.1039/C9FO02241D

15. Quan H, Zhang R. Microglia dynamic response and phenotype heterogeneity in neural regeneration following hypoxic-ischemic brain injury. Front Immunol. 2023;14:1320271. doi:10.3389/fimmu.2023.1320271

16. Khosravi M, Ghotbeddin Z, Chinipardaz S. The RNA-Binding Proteins Promote Resistance of Microglial Cells to Hypoxia. Adv Pharm Bull 2026. doi: 10.34172/apb.025.46054

17. Khosravi M, Nouri M, Mohammadi A, Mosavari N, Constable P. Preparation of immunomagnetic beads coupled with a rhodamine hydrazine immunosensor for the detection of Mycobacterium avium subspecies paratuberculosis in bovine feces, milk, and colostrum. J Dairy Sci 2021;104(6):6944-60. doi: 10.3168/jds.2020-18819

18. Woolf Z, Stevenson TJ, Lee K, Highet B, Macapagal Foliaki J, Ratiu R, et al. In vitro models of microglia: a comparative study. *Sci Rep. 2025*;15(1):15621. doi: 10.1038/s41598-025-99867-z

19. Nakagawa M, Karim MR, Izawa T, Kuwamura M, Yamate J. Immunophenotypical characterization of M1/M2 macrophages and lymphocytes in cisplatin-induced rat progressive renal fibrosis. Cells. 2021;10(2):257. doi: 10.3390/cells10020257

20. O'Bryan MK, Gerdprasert O, Nikolic-Paterson DJ, Meinhardt A, Muir JA, Foulds LM, et al. Cytokine profiles in the testes of rats treated with lipopolysaccharide reveal localized suppression of inflammatory responses. Am J Physiol Regul Integr Comp Physiol. 2005;288(6):R1744-R55. doi: 10.1152/ajpregu.00651.2004

21. Satoh S, Suzuki A, Asari Y, Sato M, Kojima N, Sato T, et al. Glomerular endothelium exhibits enhanced expression of costimulatory adhesion molecules, CD80 and CD86, by warm ischemia/reperfusion injury in rats. Lab Invest. 2002;82(9):1209-17. doi: 10.1097/01.LAB.0000029620.13097.19

22. Hirosawa N, Uchida K, Kuniyoshi K, Murakami K, Inoue G, Miyagi M, et al. Vein wrapping promotes M2 macrophage polarization in a rat chronic constriction injury model. J Orthop Res. 2018;36(8):2210-7. doi: 10.1002/jor.23875

23. Aryafar T, Amini P, Rezapoor S, Shabeeb D, Musa AE, Najafi M, et al. Modulation of radiation-induced NADPH oxidases in rat's heart tissues by melatonin. J Biomed Phys Eng. 2021;11(4):465. doi: 10.31661/jbpe.v0i0.1094

24. Zhu G, Tang Y, Liang X, Zheng M, Yang J, Zhou H, et al. Role of hypoxia-inducible factor-1 alpha in the regulation of plasminogen activator activity in rat knee joint chondrocytes. Osteoarthritis Cartilage. 2009;17(11):1494-502. doi: 10.1016/j.joca.2009.05.005

25. Helal R, Melzig MF. Determination of lysozyme activity by a fluorescence technique in comparison with the classical turbidity assay. Pharmazie 2008;63(6):415-9. doi: 10.1691/ph.2008.7846

26. Malle E, Furtmüller P, Sattler W, Obinger C. Myeloperoxidase: a target for new drug development? Br J Pharmacol. 2007;152(6):838-54. doi: 10.1038/sj.bjp.0707358

27. Rao YV, Romesh M, Singh A, Chakrabarti R. Potentiation of antibody production in Indian major carp Labeo rohita, rohu, by Achyranthes aspera as a herbal feed ingredient. Aquaculture 2004;238(1-4):67-73. doi: 10.1016/j.aquaculture.2004.04.029

28. Liu W, Rong Y, Wang J, Zhou Z, Ge X, Ji C, et al. Exosome-shuttled miR-216a-5p from hypoxic preconditioned mesenchymal stem cells repair traumatic spinal cord injury by shifting microglial M1/M2 polarization. J Neuroinflammation. 2020;17(1):47. doi: 10.1186/s12974-020-1726-7

29. Patel GK, Khan MA, Zubair H, Srivastava SK, Khushman MD, Singh S, Singh AP. Comparative analysis of exosome isolation methods using culture supernatant for optimum yield, purity and downstream applications. Sci Rep. 2019;9(1):5335. doi: 10.1038/s41598-019-41800-2

30. Dash M, Palaniyandi K, Ramalingam S, Sahabudeen S, Raja NS. Exosomes isolated from two different cell lines using three different isolation techniques show variation in physical and molecular characteristics. Biochim. Biophys. Acta - Biomembr. 2021;1863(2):183490. doi: 10.1016/j.bbamem.2020.183490

31. Francos-Quijorna I, Amo-Aparicio J, Martinez-Muriana A, López-Vales R. IL-4 drives microglia and macrophages toward a phenotype conducive for tissue repair and functional recovery after spinal cord injury. Glia. 2016;64(12):2079-92. doi: 10.1002/glia.23041

32. Tanaka S, Uehara T, Nomura Y. Up-regulation of protein-disulfide isomerase in response to hypoxia/brain ischemia and its protective effect against apoptotic cell death. J Biol Chem. 2000;275(14):10388-93. doi: 10.1074/jbc.275.14.10388

33. Duan D, Zheng K-x, Shen Y, Cao R, Jiang L, Lu Z, et al. Label-free high-throughput microRNA expression profiling from total RNA. Nucleic Acids Res. 2011;39(22):e154-e. doi: 10.1093/nar/gkr774

34. Wen X, Xiao L, Zhong Z, Wang L, Li Z, Pan X, et al. Astaxanthin acts via LRP-1 to inhibit inflammation and reverse lipopolysaccharide-induced M1/M2 polarization of microglial cells. Oncotarget. 2017;8(41):69370. doi: 10.18632/oncotarget.20628

35. Oyarce K, Cepeda MY, Lagos R, Garrido C, Vega-Letter AM, Garcia-Robles M, et al. Neuroprotective and neurotoxic effects of glial-derived exosomes. Front Cell Neurosci. 2022;16:920686. doi: 10.3389/fncel.2022.920686

36. Colvett I, Saternos H, Coughlan C, Vielle A, Ledreux A. Extracellular vesicles from the CNS play pivotal roles in neuroprotection and neurodegeneration: lessons from in vitro experiments. Extracell Vesicles Circ Nucl Acids.2023;4(1):72. doi: 10.20517/evcna.2023.07

37. Roseborough AD, Myers SJ, Khazaee R, Zhu Y, Zhao L, Iorio E, Elahi FM, Pasternak SH, Whitehead SN. Plasma derived extracellular vesicle biomarkers of microglia activation in an experimental stroke model. J. Neuroinflamm. 2023;20(1):20. doi: 10.1186/s12974-023-02708-x

38. Fitzner D, Schnaars M, Van Rossum D, Krishnamoorthy G, Dibaj P, Bakhti M, Regen T, Hanisch UK, Simons M. Selective transfer of exosomes from oligodendrocytes to microglia by macropinocytosis. J. Cell Sci. 2011;124(3):447-58. doi.org/10.1242/jcs.074088

39. Lynch S, Santos SG, Campbell EC, Nimmo AM, Botting C, Prescott A, Antoniou AN, Powis SJ. Novel MHC class I structures on exosomes. J. Immunol. 2009;183(3):1884-91. https://doi.org/10.4049/jimmunol.0900798

40. Glisovic T, Bachorik JL, Yong J, Dreyfuss G. RNA-binding proteins and post-transcriptional gene regulation. FEBS Lett. 2008;582(14):1977-86. doi: 10.1016/j.febslet.2008.03.004

41. Tao Y, Zhang Q, Wang H, Yang X, Mu H. Alternative splicing and related RNA binding proteins in human health and disease. Signal Transduct Target Ther. 2024;9(1):26. doi: 10.1038/s41392-024-01734-2

42. Rahimian R, Perlman K, Canonne C, Mechawar N. Targeting microglia–oligodendrocyte crosstalk in neurodegenerative and psychiatric disorders. Drug Discov Today. 2022;27(9):2562-73. doi: 10.1016/j.drudis.2022.06.015

43. Vermot A, Petit-Härtlein I, Smith SM, Fieschi F. NADPH oxidases (NOX): an overview from discovery, molecular mechanisms to physiology and pathology. Antioxidants (Basel). 2021;10(6):890. doi: 10.3390/antiox10060890

44. Rustenhoven J, Aalderink M, Scotter EL, Oldfield RL, Bergin PS, Mee EW, et al. TGF-beta1 regulates human brain pericyte inflammatory processes involved in neurovasculature function. J Neuroinflammation. 2016;13(1):37. doi: 10.1186/s12974-016-0503-0

45. Li JY, Boado RJ, Pardridge WM. Blood—brain barrier genomics. J Cereb Blood Flow Metab. 2001;21(1):61-8. doi: 10.1097/00004647-200101000-00008

46. Chen S-F, Pan M-X, Tang J-C, Cheng J, Zhao D, Zhang Y, et al. Arginine is neuroprotective through suppressing HIF-1α/LDHA-mediated inflammatory response after cerebral ischemia/reperfusion injury. Mol Brain. 2020;13(1):63. doi: 10.1186/s13041-020-00601-9

47. Krystofova J, Pathipati P, Russ J, Sheldon A, Ferriero D. The arginase pathway in neonatal brain hypoxia-ischemia. Dev Neurosci. 2018;40(5-6):437-50. doi: 10.1159/000496467

48. Serdar M, Kempe K, Rizazad M, Herz J, Bendix I, Felderhoff-Müser U, et al. Early pro-inflammatory microglia activation after inflammation-sensitized hypoxic-ischemic brain injury in neonatal rats. Front Cell Neurosci. 2019;13:237. doi: 10.3389/fncel.2019.00237

49. Yoon HS. Neonatal innate immunity and Toll-like receptor. Korean J Pediatr. 2010;53(12):985. doi: 10.3345/kjp.2010.53.12.985

50. Zeiss CJ. Comparative milestones in rodent and human postnatal central nervous system development. Toxicol Pathol. 2021;49(8):1368-73. doi: 10.1177/01926233211046933